Direct Numerical Simulation of Turbulent Periodic Obstacle Flow

R. Kessler* and K. S. Yang**

(Received December 16, 1996)

A direct numerical simulation (DNS) of turbulent flow in a channel with square obstacles mounted on a wall was carried out. The Reynolds number was 6820 based on the bulk velocity in the channel and the channel height. The main objective of the work was to evaluate statistical data from the time-dependent numerical solution. The influence of numerical and statistical errors on these data was examined. A comprehensive data base including 290 correlations was set up for testing and improving turbulence models for this complex, separated flow.

Key Words: Direct Numerical Simulation (DNS), Turbulence, Obstacle.

1. Introduction

Despite the progress in numerical algorithm and computer power, reliable numerical prediction of complex turbulent flows is still a challenge. Direct numerical simulations (DNS) of these turbulent flows require much computing time and cannot be applied as a standard engineering tool. Therefore, the Reynolds averaged equations or, for special cases, large eddy simulations have to be used together with appropriate turbulence models to do practical flow field predictions. However, even the most advanced turbulence models have shortcomings in predicting complex separated flows. Therefore, the further improvement of these models is one of the most important tasks in computational fluid dynamics. Statistical data derived from direct numerical simulations of turbulent flows are good tools for comparing directly closure formulae with the terms being modelled. Such DNS data bases can provide guidelines for model developers and model testing. For simple developed channel flow, such data bases were created by Mansour et al. (1988) or Gilbert and Kleiser (1991). More recently, a data base for separated flows was created by (Le et al., 1993).

The paper presents a direct numerical simulation of a turbulent channel flow over two-dimensional square obstacles. The physical problem and the numerical method are illustrated in chapter 2. In chapter 3, the mean flow is shown and compared with experiments of Dimaczek et al. (1989). Special emphasis is laid on the error estimation for the statistical data in chapter 4. The budget of Reynolds stresses is presented in chapter 5 and conclusions can be found in chapter 6.

2. Physical Problem and Numerical Method

The turbulent flow over rectangular obstacles has been studied by several authors (e. g. Tropea and Gackstatter, 1985; Dimaczek et al., 1989; Werner and Wengle, 1989). In spite of the simple cartesian geometry, the flow topology is very complex with primary and secondary separation regions around the obstacle (see streamlines in Fig. 2(a)). The computational domain is shown in Fig. 1. Its length, height and width was set to $16h$, $2h$ and $4h$ respectively, where h is the height of the square obstacle. No-slip boundary conditions were employed at the walls, and periodic boundary conditions imposed in both the homogeneous (x_3) and the streamwise direction (x_1).

* German Aerospace Center, Institute of Fluid Mechanics, D-37073 Göttingen, Germany

** Dept. of Mechanical Engineering, INHA University, Inchon, 402-751, Korea

Periodicity in the streamwise direction was chosen to avoid the expensive generation of input data and problems with appropriate outflow conditions. Moreover, the length of the computational domain could be much shorter than using in/outflow conditions. However, when applying periodicity in the x_1-direction, we actually simulate the flow in an infinitely long channel over a periodic array of obstacles rather than the flow over a single obstacle. The effect of this approach will be discussed in chapter 3. The Reynolds number based on the bulk velocity U_B in the channel and the channel height $H=2h$ was 6820.

The incompressible Navier-Stokes equations were solved by applying a finite volume method on a staggered grid. The method is of second order accuracy in space and time. The vectorized code was optimized and run on a NEC-SX3 at 1.5 GFLOPS. A detailed description of the numerical scheme is given in Yang and Ferziger (1993). Two runs on two non-equidistant grids ($204\times72\times36$ and $384\times168\times72$) were performed to check out the influence of the numerical resolution. The wall nearest grid points of the fine grid are located typically one wall unit apart the wall.

The numerical simulation and the data evaluation were done in succession. After an initial transient period the velocity and pressure fields were stored every 80th time step during an interval of 130 time units (h/U_B). This time interval corresponds to more than 9 flow-through times. On completion of the simulation all statistical data were calculated by averaging over the homogeneous direction (x_3) and the time interval mentioned above.

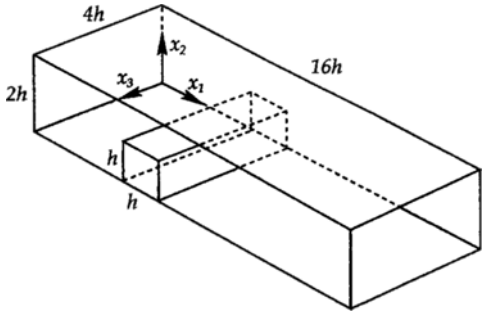

Fig. 1 Geometry of computation domain.

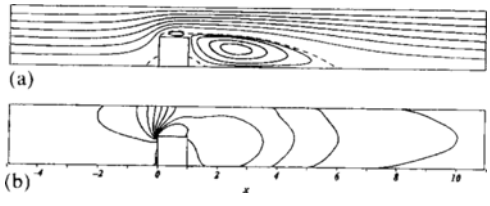

Fig. 2 (a) Streamlines and (b) isobars of the mean flow.

3. Mean Flow Results

The calculated streamlines of the time averaged flow are shown in Fig. 2(a). The separation and reattachment points are connected by dashed lines. Three primary recirculation zones at the front, top, and rear face of the obstacle and one secondary recirculation can be seen. Two of the recirculation zones are connected by a free stagnation point near the trailing edge of the obstacle. Isolines of the pressure are plotted in Fig. 2(b). The pressure drop caused by the obstacle can be observed up to $3h$ upstream of the constriction.

The topological structure of the instantaneous flow field is completely different from that of the averaged flow field. This is shown in Fig. 3 by plotting regions of negative streamwise velocity U_1. In Fig. 3(a), (b) these regions are plotted for the midplane of the computational box ($z=2h$) at different times. Various points of separation and reattachment and their temporal variations illustrate the complex time-dependent structure of this flow. Small regions of back flow can be observed up to $9h$ downstream the obstacle at the

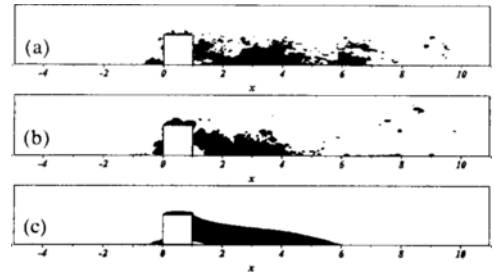

Fig. 3 Regions of negative streamwise velocities U_1 from instantaneous flow fields at $z=2h$ and $t_1=72.98$ (a) and $t_2=77.04$ (b) and averaged flow field (c).

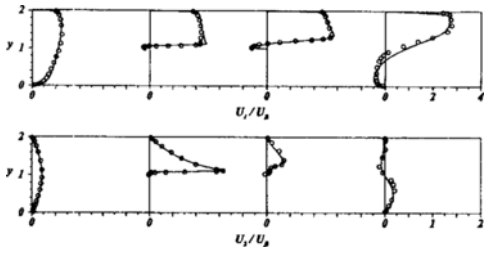

Fig. 4 Profiles of normalized velocity components U_1 and U_2 at $x=-1.2h$, $x=0.08h$, $x=0.48h$ and $x=2h$;— DNS, ◦ experimental data of Dimaczeck et al. (1989).

lower wall, in the core flow of the channel, and even at the upper wall. This is a consequence of the high turbulence level generated by the shear layer above the obstacle. By applying the average process, the flow structure is drastically simplified, and only two regions of the back flow remain (Fig. 3(c)). These pictures illustrate the loss of information about the flow structure by the Reynolds averaging.

Profiles of the mean velocities at four cross sections are shown in Fig. 4. Upstream of the obstacle, the flow is accelerated in the upper part of the channel, caused by the displacement effect of the obstacle. This results in an asymmetric U_1 profile and positive U_2 values at $x=-1.2h$. The development of a shear layer with a thin recirculation zone above the obstacle can be seen in the second and third profiles ($x=0.08h$ and $x=0.48h$) of Fig. 4. The flow around the leading corner of the obstacle leads to a pronounced peak in the U_2 profile at $0.08h$. The forth section is located downstream the obstacle and shows the backflow of the large recirculation zone at $x=2h$.

Experimental data of Dimaczek et al. (1989) are included in the profiles of Fig. 4. This experiment was performed at a Reynolds number of 84000 with a fully developed channel flow upstream of the obstacle. Although the experimental flow conditions are quite different from those applied in our simulation, the predicted and measured data are in almost perfect agreement at the sections upstream and above the obstacle. The principle flow phenomena seem to be similar in both the predicted and the measured flow and may be only little affected by Reynolds number effects or the upstream flow. At the fourth section, one h downstream the obstacle, the predicted U_1 profile slightly differs from the measured values. The predicted shear layer expands more rapidly than the measured one, which may be attributed to the different Reynolds number of simulation and experiment.

4. Error Estimation

Experimental data for obstacle flows at low Reynolds numbers are rare. Moreover, no experimental data are available for pressure correlations, dissipation or other higher order terms. Therefore, an error estimation is essential for the assessment of the calculated data. The data derived by the statistical evaluation can be affected by statistical errors, and numerical errors of the simulation or the evaluation process.

4.1 Statistical errors

The statistical errors decrease with an increasing number of statistically independent data used for the averaging process. We applied the data of about 800 time sheets for the evaluation. A second evaluation was performed with a reduced averaging interval (250 time sheets) to check out the influence of the statistical errors.

The mean flow is less affected by statistical errors. Even in regions with a high turbulence level, the disagreement did not exceed 5% for the mean values. A different behaviour can be observed for some higher order correlations. For example, the profiles of the dissipation rate ε and the turbulent diffusion $T_k=(u_iu_iu_k)_{,k}/2$ of the turbulent kinetic energy k are shown in Fig. 5 calculated with averaging intervals ΔT_{av} of 130 and 40 time units, respectively. The dissipation is smooth and little difference can be seen between the two curves. By contrast, the profiles of the triple correlations are superposed by fluctuations. High amplitudes of these fluctuations occur in regions with high turbulence levels. An increasing time averaging interval ΔT_{av} results in a decrease of the waviness.

A possible explanation for this behaviour can be found in the different time scales of small and

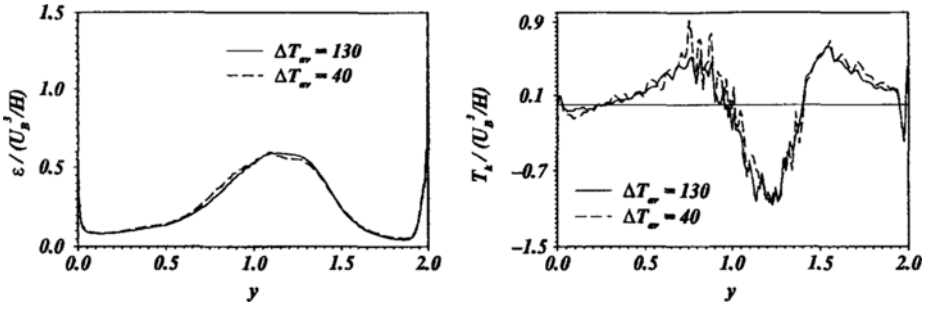

Fig. 5 Profiles of the normalized dissipation rate ε and the turbulent diffusion of k for different averaging intervals ΔT_{av} at $x=3h$.

large scale elements. Mainly small scale motions contribute to the dissipation rate. The time scale of these elements is smaller than the time difference between two succeeding time sheets. Therefore, all the data are statistically independent and small statistical errors can be achieved for the dissipation rate. The time scale for the large turbulent elements exceeds the time difference between two succeeding time sheets. Therefore, the number of statistically independent data is reduced, and the larger statistical errors occur if a large scale motion contributes to a correlation.

Statistical errors deteriorate the smoothness of some correlations, but generally they do not change the principal shape of the profiles. To ensure smooth profiles for all correlations, the time averaging interval of the present simulation should be extended by a factor of 5. Unfortunately, this was not possible because the cpu time resources were limited.

4.2 Numerical errors

An extra run was performed with approximately half the grid points of the fine grid DNS in each direction. A complete evaluation of the resulting data was carried out subsequently. Comparison of the results of both simulations can give a rough idea which parts of the results are mostly affected by an insufficient numerical resolution.

Four flow quantities were shown in Fig. 6 to illustrate the results of the comparison. Profiles were plotted at the midpoint of the obstacle ($x=0.5h$) and downstream of the obstacle ($x=3h$) near the centre of the large recirculation zone.

The profiles of the mean velocities of coarse and fine grid simulations agree well in the whole computational domain with the exception of a thin separation region at the top wall of the obstacle (Fig. 6(a)). For the coarse grid simulation, the width of the shear layer grows more rapidly. In contrast to the experimental results and the fine grid solutions, the flow reattaches near the trailing edge of the obstacle. Profiles of turbulent fluctuations, represented by the turbulent kinetic energy k can be seen in Fig. 6(b). Differences of less than 10% can be observed, mostly concentrated near the separation zones. More pronounced deviations can be detected in Fig. 6(c) for the dissipation rate, which is underpredicted throughout the flow field by the coarse grid simulation. Differences up to 60% occur mainly in the regions of separation zones. Astonishingly, many of the higher order correlations were well predicted even by the coarse grid simulation. An example is given in Fig. 6(d). Profiles of the turbulent diffusion T_k resulting from the coarse and fine grid simulation are close together even in the "critical" region around the obstacle.

Two conclusions can be drawn from the comparison. Firstly, the numerical resolution is clearly insufficient near the top wall of the obstacle for the coarse grid simulation and probably also for the fine grid DNS. The remaining flow field seems to be well resolved at least with the fine grid simulation, and numerical errors seem to have negligible effects on the correlations away from the obstacle. Secondly, some of the turbulent quantities, above all the dissipation rate, are strongly affected by numerical errors, whereas

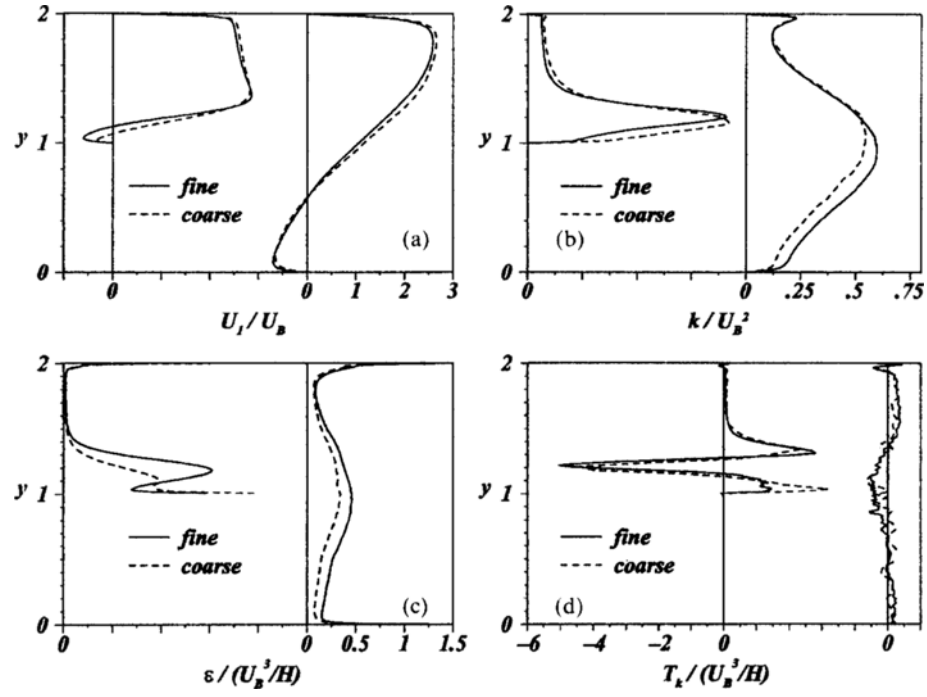

Fig. 6 Comparison of coarse and fine grid solutions, (a) mean velocity U_1, (b) turbulent kinetic energy k, (c) dissipation rate ε and (d) turbulent diffusion of k at $x=0.5h$ and $x=3h$.

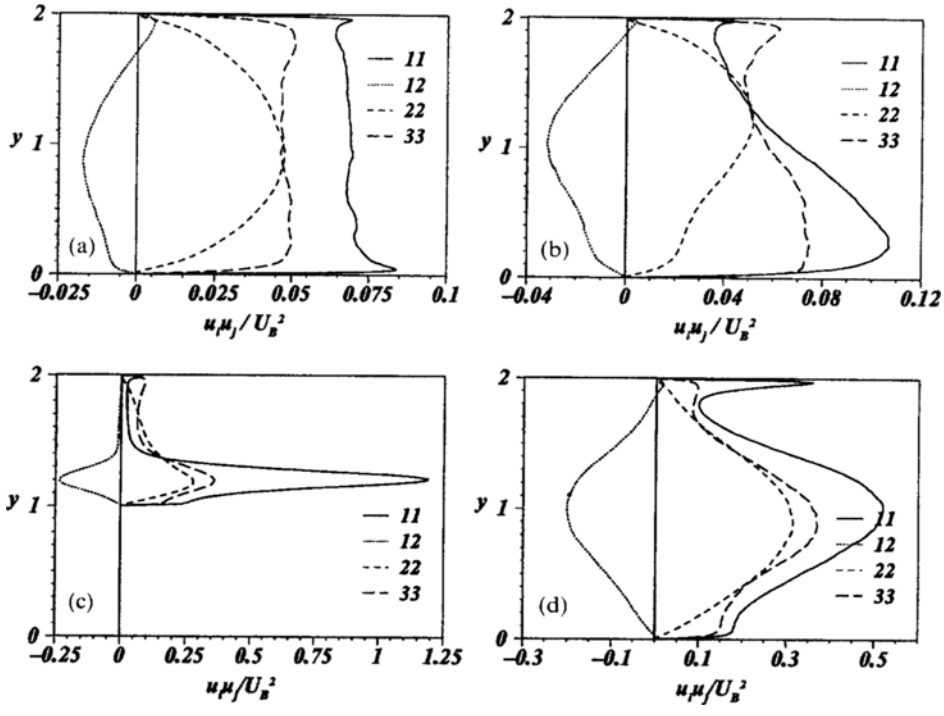

Fig. 7 Reynolds stresses at various cross sections, (a) $x=-2h$, (b) $x=-0.5h$, (c) $x=0.5h$ and (d) $x=3h$.

other correlations are less sensitive and can be well predicted even by the coarse grid simulation. The differences between coarse and fine grid solutions were assumed to be an upper bound for the numerical errors of the fine grid DNS.

5. Statistical Quantities

5.1 Reynolds stresses

Predicted Reynolds stresses at four different sections are shown in Fig. 7. At the first section, $2h$ upstream the obstacle, the flow is characterized by a decaying turbulence. The asymmetry is nearly balanced, but all turbulent fluctuations are one order of magnitude higher than the values known from a fully developed channel flow. At the next section ($x=-0.5$) flow in the upper part of the channel is strongly accelerated due to the displacement effect of the obstacle. As a consequence, the streamwise fluctuations u_1u_1 decrease below the values of the wall normal component u_2u_2. Above the obstacle strong peaks of all components of the Reynolds stress tensor produced by the shear layer can be seen in Fig. 7 (c) ($x=0.5h$). Whereas the streamwise fluctuations dominate in the shear layer region, the spanwise and wall-normal fluctuations exceed them in the core region above. The kink in the curves of all normal stresses in the vicinity of the obstacle wall was also observed in related experiments (Dimaczek et al., 1989), and is therefore attributed to the physical effects rather than to a numerical deficiency. The profiles displayed in the last figure are typical for separated flows. Similar shapes can be found in backward facing step flows. However, the turbulence level of the obstacle flow is clearly higher than that of many other separated flows.

5.2 Budget for Reynolds stresses

Our evaluation includes all terms appearing in the transport equations for the Reynolds stresses u_iu_j, the dissipation rate ε, and the vorticity correlation $\omega_i\omega_i$. We restrict ourselves in presenting budgets of the Reynolds stresses u_iu_j at two cross section. The transport equation for these correlations reads

$$\frac{D(u_iu_j)}{Dt}=P_{ij}+T_{ij}+D_{ij}+\pi_{ij}+\phi_{ij}-\varepsilon_{ij}$$

with the production P_{ij}, the turbulent diffusion T_{ij}, the molecular diffusion D_{ij}, the pressure diffusion π_{ij}, the pressure strain term ϕ_{ij}, and the dissipation ε_{ij}. For statistically steady flows, the substantial derivative on the left hand side reduces to the convective transport term $-C_{ij}$. The complete formulae for all terms can be found for example in Mansour et al. (1988). The budgets of the Reynolds stresses u_iu_j at $x=0.5h$ are plotted in Fig. 8. At this section, the correlations are mainly determined by the thin shear layer above the obstacle. Fig. 8(a) shows the dominating role of the production term P_{11} in the region of this shear layer. The pressure strain term ϕ_{11} acts as a main sink term, and transfers the energy to the other normal stress components. The turbulent diffusion term T_{ij} transports the streamwise stress from the centre of the shear layer to its edges. Outside the shear layer, the magnitude of all correlations drop down by more than an order of magnitude.

The pressure strain terms ϕ_{22} and ϕ_{33} are the main production terms for the other normal Reynolds stresses at this section (Fig. 8(b), (c)). In the region of the shear layer, these terms are balanced by the convective transport, the viscous dissipation and, in the case of u_2u_2, by the negative production term P_{22}.

The residuals of the budget of all Reynolds stresses come up to 20-40% of the respective production term in the high shear region. The shape and sign of the residuals equal that of the related viscous dissipation term. This fact and the error estimation presented in chapter 4.2 lead to an assumption that strong underprediction of the viscous dissipation is the main reason for the defects in the balances.

The behaviour of the budgets at the upper channel wall is almost identical to that in a developed channel flow. A detailed view of the budgets near the top wall of the obstacle can be seen in Fig. 8(e)-(h). The meaning of the symbols corresponds to those of the upper part of the figure. The redistribution term π_{11} (Fig. 8(e)) and the turbulent diffusion term T_{22} (Fig. 8(f))

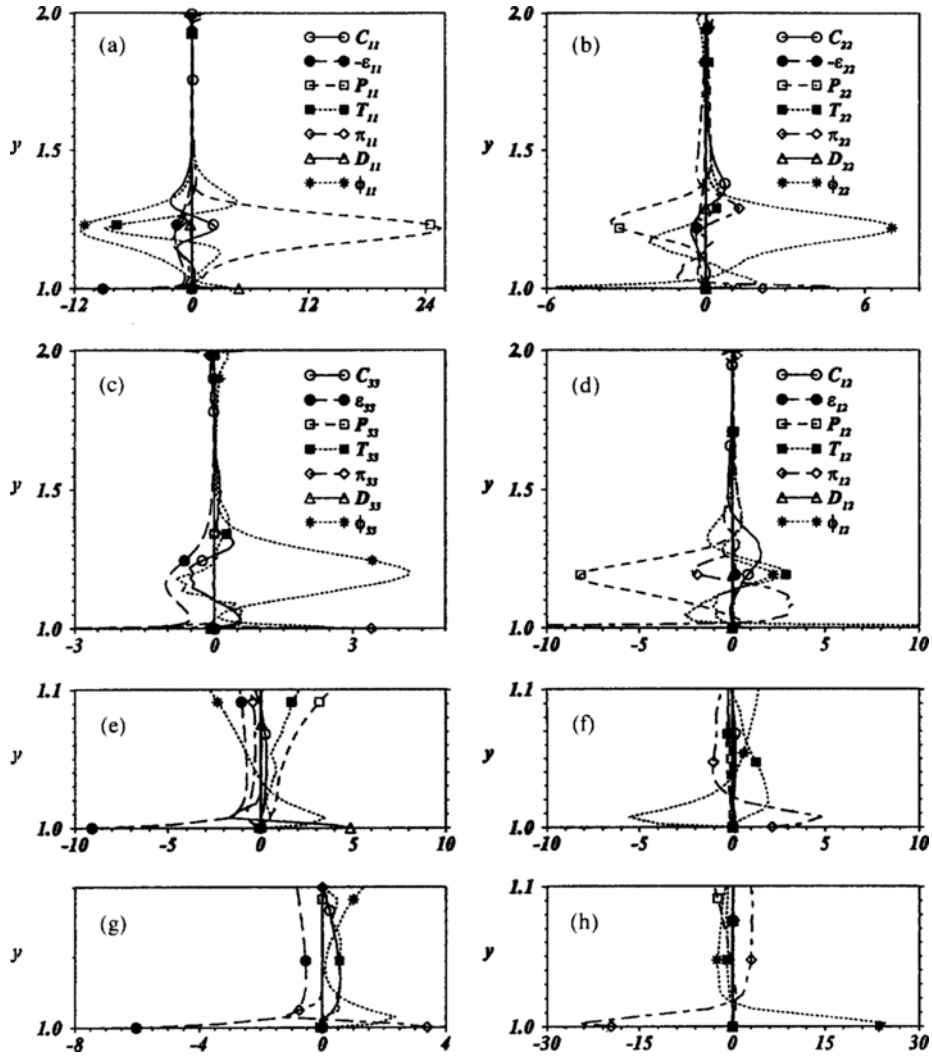

Fig. 8 Budgets of the Reynolds stresses at $x=0.5h$; u_1u_1 (a, e), u_2u_2 (b, f), u_3u_3 (c, g) and u_1u_2 (d, h).

show a maximum near the wall. These are the most pronounced differences compared to the behaviour of a fully developed channel flow.

The budgets of all Reynolds stress components at the section $x=3h$ are shown in Fig. 9. This cross section is located near the centre of the large separation region downstream the obstacle. Here, the energy containing turbulent elements and the corresponding turbulent time scales are larger than those above the obstacle. As a consequence, the statistical errors are larger at this section which results in wiggles in the curves of most correlations.

The profiles of all terms of the budgets look qualitatively similar to those reported by Le and Moin (1993) for the recirculating flow downstream a backward facing step. The production of turbulence is biggest in the middle of the channel represented by the term P_{11} (Fig. 9(a)). The pressure strain term again acts as a sink for the streamwise component of the Reynolds normal stress, and is the main "production" term for the other normal components. The turbulent diffusion terms T_{ij} distribute the energy of all components from the centre of the shear layer to near wall regions. The budget of the Reynolds shear

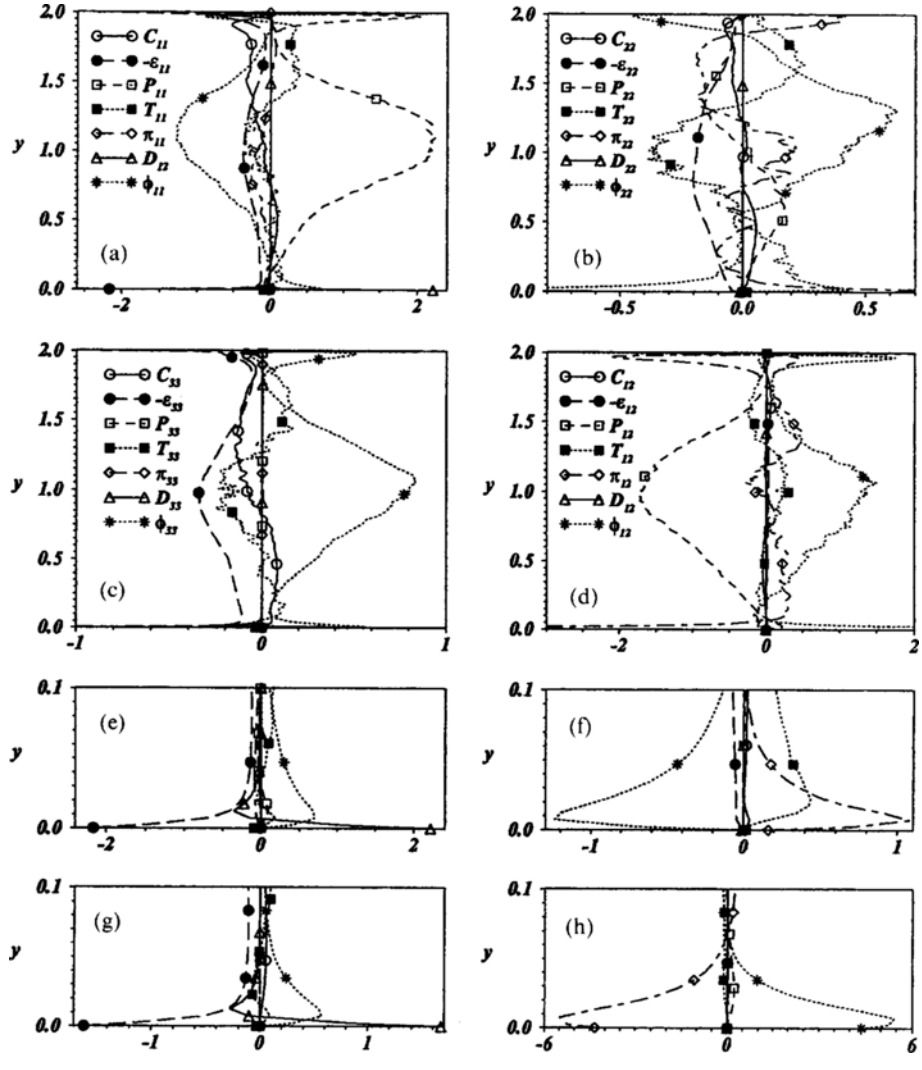

Fig. 9 Budgets of the Reynolds stresses at $x=3h$; u_1u_1 (a, e), u_2u_2 (b, f), u_3u_3 (c, g) and u_1u_2 (d, h).

stress u_1u_2 is dominated by the balance of the production and pressure strain term. Contrary to the section at $x=0.5$, the turbulent diffusion T_{12} plays only a minor role. The residuals of the budgets does not exceed 5–10% of the respective dominant terms, indicating small numerical errors at this section. The near wall behaviour of the correlations at $x=3h$ (Fig. 9(e)–(h)) are similar to these above the obstacle with a different scaling due to the different wall shear velocity at both sections.

The production terms of the Reynolds normal stresses fall below zero in certain parts of the flow field. To illustrate this phenomenon, we mark regions of negative values of the production term of the turbulent kinetic energy $P_k=u_iu_k\partial U_i/\partial x_i$ in Fig. 10. The energy transfer from the mean flow to the turbulent fluctuations, which is a normal situation in turbulent flows, is equivalent to a positive value of P_k. However, a negative production term P_k indicates the reverse situation with an energy transfer from the turbulent motion to the mean flow. Regions of negative production can be seen at the front and rear walls and parts of the top wall of the obstacle. These zones partly coincide with the the temporal appearance of

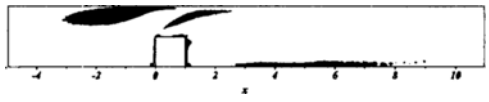

Fig. 10 Regions of negative production term P_k of the turbulent kinetic energy $\frac{1}{2}u_iu_i$.

separation or reattachment points at the adjacent wall. Moreover, negative production can be observed upstream the obstacle where the mean flow is accelerated, and also on the upper edge of the shear layer above the obstacle.

6. Summary and Conclusions

The direct numerical simulation of a turbulent channel flow over a square obstacle was presented. Around the obstacle, the predicted mean velocity profiles are in very good agreement with experimental data, although Reynolds number and upstream flow conditions applied for the simulation are quite different from those realized in the experiment.

By comparing the coarse and fine grid solutions, we found the numerical resolution of the present DNS to be sufficient upstream and downstream the obstacle. Above the obstacle, not all the physically relevant scales are resolved, and more grid points would be needed to reduce the numerical errors in this region.

The statistical error introduced by the finite time average interval is highest in the centre of the shear layer, where the turbulence level is high. Dissipation is little affected by this error, whereas turbulent diffusion, pressure diffusion, and the convective transport term are strongly influenced by statistical errors.

An estimation of the effect of numerical errors on statistical data was derived by comparing results of the coarse and fine grid solutions. The dissipation term was found to be most sensitive to numerical errors of the simulation. However, the mean flow and also some higher order correlations can be calculated satisfactorily even with a coarse grid simulation.

Budgets of the Reynolds stresses were presented at two cross sections. The residue of the budgets is mainly explained with an underprediction of the viscous dissipation. Extended regions of negative turbulence production are localized near separation or reattachment points and at the edge of the thin shear layer.

The data base derived from the present simulation will be a helpful tool for testing and improving advanced turbulence models. The obstacle flow itself remains a challenge for both direct numerical simulations and turbulence modellers.

Acknowledgement

The authors gratefully acknowledge the financial support of the Deutsche Forschungsgemeinschaft (DFG) and the Korea Science and Engineering Foundation (KOSEF) by a 1995 international collaborative research project. The authors also thank the SERI supercomputer center in Korea for providing access to the CRAY C90 for the present work.

References

Dimaczek, G., Kessler, R., Martinuzzi, R. and Tropea, C., 1989, "The Flow over Two-Dimensional, Surface-Mounted Obstacles at High Reynolds Numbers," *Proc. of 7th Symposium on Turbulent Shear Flows*, Stanford, Aug. 21-23.

Gilbert, N. and Kleiser, L., 1991, "Turbulence Model Testing with the Aid of Direct Numerical Simulation Results," *Proc. of 8th Symposium on Turbulent Shear Flows*, Paper 26-1, Munich, Sept. 9-11.

Le, H., Moin, P. and Kim, J., 1993, "Direct Numerical Simulation of Turbulent Flow over a Backward-Facing Step," *Proc. of 9th Symposium on Turbulent Shear Flows*, Paper 13-2, Kyoto, Aug. 16-18.

Mansour, N. N., Kim, J. and Moin, P., 1988, "Reynolds-Stress and Dissipation-Rate Budgets in a Turbulent Channel Flow," *J. Fluid Mech.*, Vol. 194, pp. 15~44.

Tropea, C. and Gackstatter, R., 1985, "The Flow over Two-Dimensional Surface-Mounted Obstacles at Low Reynolds Numbers," *J. Fluid Eng.*, Vol. 107, pp. 489~494.

Werner, H. and Wengle, H., 1989, "Large -Eddy Simulation of Turbulent Flow over a Square Rib in a Channel," *Proc. of 7th Symp. on Turbulent Shear Flows*, Stanford, Aug. 21-23.

Yang, K. S. and Ferziger, J. H., 1993, "Large -eddy simulation of turbulent obstacle flow using a dynamic subgrid-scale model," *AIAA Journal*, Vol. 31, pp. 1406~1413.